Storm surge modelling in the Strait of Georgia

Nancy Soontiens, Susan Allen, Doug Latornell, Kate Le Souëf, Idalia Machuca,

Youyu Lu, Keith Thompson, Jean-Philippe Paquin, Vasily Korabel

December 2, 2014

Abstract

The Strait of Georgia is a large, semi-enclosed body of water between Vancouver Island and the mainland of British Columbia connected to the Pacific Ocean via the Strait of Juan de Fuca at the south and Johnstone Strait at the north. During the winter months, coastal communities in the Strait of Georgia are at risk to flooding caused by storm surges, a natural hazard that can occur when a strong storm coincides with high tide. This investigation produces storm surge hindcasts using a three-dimensional numerical ocean model for the Strait of Georgia and the surrounding bodies of water (Strait of Juan de Fuca, Puget Sound, and Johnstone Strait) collectively known as the Salish Sea. The numerical model employs the Nucleus for European Modelling of the Ocean (NEMO) architecture in a regional configuration. The model is evaluated through comparisons of tidal elevation harmonics and storm surge water levels with observations. Important forcing factors contributing to storm surges have been assessed, finding that the surge entering the domain from the Pacific Ocean contributes most significantly. Comparisons between simulations with high resolution and low resolution atmospheric forcing further emphasize this point. In addition, local wind patterns cause a slight increase in surge amplitude on the mainland side of the Strait of Georgia when compared to the Vancouver Island coastal areas during a major wind storm on Dec 15, 2006. Generally, surge amplitudes are found to be greater within the Strait of Georgia when compared to amplitudes in the Strait of Juan de Fuca.

1   Introduction

The Strait of Georgia is a strongly stratified, semi-enclosed body of water located between Vancouver Island and the mainland of British Columbia. It is part of a larger system of waterways collectively known as the Salish Sea and is connected to the Pacific Ocean via the Strait of Juan de Fuca and Johnstone Strait

(Figure 1). It is on average 220 km in length and 28 km wide and its maximum depth is 420 m (Thomson, 1981). At its southern end, the Strait of Georgia is connected to the Strait of Juan de Fuca through several passages, the largest being Haro Strait. The San Juan and Gulf Islands are scattered throughout these passages where complex bathymetry and steep topographic slopes induce vigorous tidal mixing. Many rivers feed fresh water into the Salish Sea system, the most significant source being from the Fraser River. Mixed diurnal and semi-diurnal tides are found throughout most of the Salish Sea but a semi-diurnal amphidrome is present nearby Victoria, where the tides are mainly diurnal (Thomson, 1981). This system is home to several large coastal communities, such as Vancouver and Victoria, serves as a waterway for commercial traffic and recreational use, and supports a large and active fishing industry.

Several features related to the physical oceanography of this region render it a challenge to model numerically. The outflow from the Fraser River in the late spring is the primary source of fresh water within the Strait of Georgia and leads to large vertical density gradients in the summer months (Thomson, 1981). Additionally, strong tidal mixing through the San Juan and Gulf Islands produces horizontal density gradients that separate the saline waters of the Strait of Juan de Fuca and the fresher water of the Strait of Georgia. It is important to accurately represent the vertical mixing in this region as it sets the rate of export of fresh water through estuarine circulation (Masson and Cummins, 2004). The strong and fast tidal currents through the narrow channels of the north, such as Discovery Passage and Johnstone Strait, set a fairly restrictive time step and impose a particular challenge for numerical models. Yet, several modelling efforts for this region exist, ranging in choices of grid structure, mixing parametrizations, and domain size and extent.

Early work by Crean et al. (1988a,b) and Stronach et al. (1993) resulted in a series of models covering the Strait of Juan de Fuca, the Strait of Georgia, and Puget Sound using a finite difference discretization of the equations of motion. A barotropic version of their model was used to reproduce storm surge water level elevations with reasonable accuracy, however, this barotropic version did not include the effects of fresh water entering the system from rivers. Later, a baroclinic version of their model examined residual circulation and fresh water flushing rates (Stronach et al., 1993; Marinone et al., 1996). This early work pointed to an important connection between the model's bottom friction parametrization and the location and amplitude of the M_2 amphidrome. They found that a local increase in the bottom friction coefficient, especially in the area of Haro Strait, was necessary in order to adequately reproduce the observed M_2 tidal amplitudes and phase lags in the Strait of Georgia (Stronach et al., 1993). Without local adjustments to the bottom friction their M_2 amplitudes were too high in the Strait of Juan de Fuca and too low in the Strait of Georgia. Other

studies over a similar domain, such as the barotropic finite element model of Foreman et al. (1995), have avoided local increases in bottom friction. Foreman et al. (2004) used data assimilation techniques to study M_2 tidal dissipation without local changes to the bottom friction in a two-dimensional finite element model that did not include baroclinic effects.

More recently, modelling studies have focused on baroclinic features. Masson and Cummins (2004) used the Princeton Ocean Model (POM) in a regional mode to examine the seasonal variability of deep water properties in the Strait of Georgia noting a strong sensitivity to vertical mixing over the sills. This model employed a sigma or terrain-following vertical coordinate system leading to spurious diapycnal mixing since, numerically, the lateral mixing is computed on sigma levels which may intersect isopycnals in the presence of steep topography. A finite volume model on an unstructured grid by Yang and Khangaonkar (2010) involved a truncated domain with an open boundary in the northern Strait of Georgia, where under predictions in the M_2 tidal phase over most of their domain were suggested to be caused by an inaccurate representation of the tides at their northern boundary. Sutherland et al. (2011) employed the Regional Ocean Modelling System (ROMS) to study estuarine circulation in the Salish Sea with a model domain that extended outside the Strait of Juan de Fuca into the Pacific Ocean and up to the northern Strait of Georgia and noted that their semi-diurnal amplitudes were generally too low. An updated version of this model produced high temperatures in the Strait of Juan de Fuca, suggesting too little mixing within the Salish Sea (Giddings et al., 2014). Smaller domains have also been considered, notably, the passageways through the Discovery Islands north of the Strait of Georgia have been modelled baroclinically by Foreman et al. (2012) with the Finite Volume Coastal Ocean Model (FVCOM) pointing to difficulties in reproducing baroclinic currents on their grid. Accurate reproduction of observed tidal amplitudes and phases and appropriate treatment of mixing is a recurring difficulty in modelling of this region.

Many coastal communities in the Strait of Georgia are at risk to flooding and property damaged caused by storm surges, a natural hazard arising from the combination of a strong wind storm and high tide. The low atmospheric pressure associated with a storm acts as an inverse barometer elevating the sea level. This effect in combination with strong winds pushing water up against the coast can cause flooding, particularly if the storm occurs during an unusually high tide. There can also be a small contribution to increased sea level due to the thermal expansion of water during warmer years set by the El Nino Southern Oscillation (ENSO) (Abeysirigunawardena et al., 2011).

Communities in the Strait of Georgia are particularly susceptible to storm surges in the winter months when there is an increased propensity for storms and a higher mean sea level caused by southeasterly winds

and geostrophic adjustment (Danard et al., 2003). In the summer months, the wind direction changes to northwesterly and mean sea level is lower. In British Columbia waters, the largest tidal ranges occur in June and December at the summer and winter solstices (Thomson, 1981). The highest water levels are observed in the winter around the perigean spring tide or "King" tide, when the sun and moon are aligned with the Earth and the moon is at its perigee. As such, storm surges in the Strait of Georgia are typically observed between November and February (Forseth, 2012). Flooding caused by a storm surge is most likely to occur during a high spring tide (Abeysirigunawardena et al., 2011).

Coastal communities can prepare for and respond to storm surge hazards using predictions from storm surge models to determine if flooding conditions are probable. Like coastal ocean models, some of the complexity of a storm surge model depends on the properties of the geographic location of interest. In shallow regions, it is important to include the effects of wetting and drying which allows grid cells to alternate between land and water depending on the modelled sea surface height and depth (Hubbert and McInnes, 1999; Weisberg and Zheng, 2006). Other regions require modelling over a very large domain since non-local effects from the open sea may influence surge propagation (Weisberg and Zheng, 2006; Lane and Walters, 2009). Such large domains typically use nested or unstructured grids to resolve the details of complicated coastlines. Appropriate treatment of rivers (Flather, 1994), accurate bathymetry and the inclusion surface waves (Xu et al., 2010) have also been identified as important issues. Most of these models neglect the effects of stratification, either by treating the ocean as a constant temperature and salinity or by using a two-dimensional depth-averaged set of equations, an assumption that is assumed to be valid. Further, an accurate representation of the meteorological conditions at the ocean surface is important.

Storm surge modelling in the Strait of Georgia dates back to Crean et al. (1988a) in a barotropic finite difference model. Their work is highlighted in reviews of storm surges in Canadian waters (Murty et al., 1995; Danard et al., 2003). Compared to eastern Canada (Gray et al., 1984; Bernier and Thompson, 2006; Bobanović et al., 2006; Bernier and Thompson, 2007, 2010), relatively little has been published on storm surge modelling on the west coast of Canada in recent years. A statistical overview of past surge events in British Columbia waters suggests an increase in extreme water level events during warm ENSO periods (Abeysirigunawardena et al., 2011).

This article presents the development of a three-dimensional numerical ocean model for the Strait of Georgia and its accuracy in simulating storm surge hindcasts. This baroclinic model includes the effect of stratification and rivers, however, wetting and drying is not represented. Model evaluation has focused on regions where the near-coast slopes are steep and so wetting and drying effects are believed to be unimportant.

4

A detailed overview of the model configuration and domain including a description of the ocean model configuration is provided in section 2. This section also describes open and surface boundary conditions as well as choices in grid structure and mixing parametrizations. Next, section 3 presents an evaluation of model performance through comparisons of tidal amplitudes and phases with observations. The model's accuracy in producing storm surge hindcasts is also assessed in section 4. Finally, a summary and discussion of future research goals is provided in section 5.

2   Model Configuration

We have used the Nucleus for European Modelling of the Ocean (NEMO) framework in its regional configuration (Madec et al., 2012) to develop an ocean model for the Strait of Georgia and Salish Sea. NEMO is a highly modularized tool used for studying ocean physics, ocean-ice interactions, and the bio-geochemical properties of the ocean. NEMO's ocean core solves the three-dimensional hydrostatic equations of motion for an incompressible fluid under the Boussinesq approximation on a structured computational grid. Although not used in the present work, NEMO's options for grid nesting and bio-geochemical coupling make it a useful tool for studying the complex physics and bio-geochemical interactions within the Strait of Georgia. This work focuses on validating the physical set up of the Salish Sea model, in particular, determining appropriate forcing and boundary conditions for accurate reproduction of tidal amplitudes and phases as well as storm surge elevations. Future work will include bio-geochemical coupling and data assimilation.

The modelled domain extends from the Strait of Juan de Fuca to Puget Sound to Johnstone Strait as shown in Figure 1. Bathymetry from the Cascadia physiography data set (Haugerud, 1999) was smoothed to limit large changes in depth across grid cells, so that $\Delta h/\bar{h} \leq 0.8$, where Δh is the difference in depth between two adjacent grid cells and $\bar{h}$ is their average depth. For model stability, additional smoothing at the Strait of Juan de Fuca western boundary was imposed to achieve constant depth across the first ten grid cells. As depicted in Figure 1, the numerical grid is rotated $29°$ counter-clockwise of North in order to maintain computational efficiency since currents within the Strait of Georgia are mainly aligned with this rotated axis.

The curvilinear orthogonal numerical grid has been divided into 398 by 898 by 40 grid cells, which results in an almost uniform horizontal resolution with grid spacing approximately 440 m by 500 m. The 40 vertical z-levels were stretched gradually in order to achieve higher resolution in the surface layer, with 1 m vertical grid spacing down to about 10 m in depth. Below 10 m the grid was stretched to a maximum grid spacing

of 27 m at the lowest layer. At the bottom boundary, partial z-levels were utilized in order to limit large changes in bathymetry across grid cells (Madec et al., 2012).

In addition to the equations of motion, a prognostic equation for the sea surface height is solved at each time step. The inclusion of the sea surface height equation requires a fairly restrictive time step due to the presence of high speed surface gravity waves. As such, the split-explicit time stepping algorithm is employed, where the free surface and barotropic equations are solved with a smaller time step than that used for the other variables. The model time step and barotropic time step are 10 s and 2 s respectively. Small vertical grid spacing and large vertical velocities in the Boundary Pass and Haro Strait region impose a fairly restrictive time step through the vertical CFL condition.
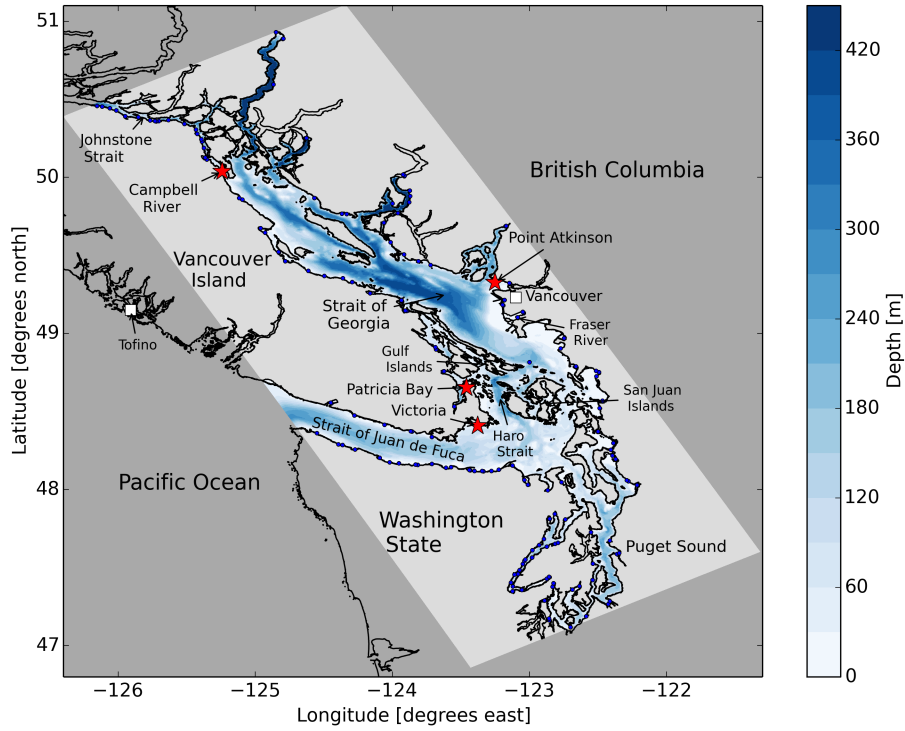

Figure 1: Model domain (highlighted area) including bathymetry, rivers (blue circles), and storm surge locations of interest (red stars).

The model includes two open boundaries that connect to the Pacific Ocean, the western boundary of the Strait of Juan de Fuca as well as Johnstone Strait at the north, both of which are forced with eight tidal constituents (K_1, O_1, P_1, Q_1, M_2, K_2, N_2, S_2), temperature and salinity climatologies, and the sea surface height anomaly. Tidal heights and currents at grid points along the Juan de Fuca boundary were extracted from Webtide, an online web prediction model for the northeast Pacific Ocean, which is

based on work by Foreman et al. (2000). The Johnstone Strait boundary was forced with current and elevation tidal harmonics measured and calculated by Thomson and Huggett (1980) for the major M_2 and K_1 constituents. Additionally, O_1 and S_2 elevation harmonics from their measurements were employed. The remaining constituents were extrapolated from Webtide. At the western boundary, the tidal elevation and currents forcing parameters were tuned for a good match with observations at locations within the Strait of Georgia, including Point Atkinson, Gibsons Landing, Winchelsea and Halfmoon Bay. At the northern boundary, the tides were tuned for good matches at Yorke Island and Kelsey Bay. Further details on the tuning are provided in Appendix A.

Temperature and salinity at the Juan de Fuca boundary were taken from a weekly climatology which was created from results from a model covering the Salish Sea and the west coast of Vancouver Island (Masson and Fine, 2012). Their results, originally on s-levels were interpolated onto z-levels and then onto the NEMO horizontal grid. To prepare the climatology all years (1995-2008) were averaged and results, approximately every 15 days, were interpolated to a weekly climatology. The model is relaxed to the forced temperature and salinity over the 10 grid points (about 5km) closest to the open boundaries, using a flow relaxation scheme (Engedahl, 1995).

Sea surface height at the mouth of Juan de Fuca was set using values from the Tofino tide gauge which is outside of but close to the western boundary of the model domain. A monthly climatology was produced using daily averages from 2000-2010, binning them by month, averaging and setting the yearly mean to zero. For the storm surge simulations, hourly variations in sea surface height were used. These values are the Tofino tide gauge values, de-tided and with the zero reset as for the climatology. The storm surge simulations also used the sea surface height anomaly from Port Hardy, forced at the northern boundary in Johnstone Strait. The tidal forcing and sea surface height was applied to the barotropic velocity forcing with the NEMO Flather scheme (Flather, 1994; Madec et al., 2012). At the west, the baroclinic velocities at the boundary were set equal to the values inside the boundary (zero-gradient boundary conditions). This scheme is not part of core NEMO 3.4, the version used here. Zero gradient conditions were chosen because the baroclinic velocity at the mouth of Juan de Fuca is primarily estuarine and thus set by density variations between inside and outside the domain. At the north baroclinic velocities were set to zero.

At coastal boundaries, the partial slip boundary condition, an approximation to no slip, is used. Partial slip allows one to include the frictional effects of lateral boundaries without the restrictive resolution required to represent the lateral boundary layer under no slip conditions. A lateral eddy viscosity of 20 m^2 s^{-1} parametrizes horizontal friction and a lateral eddy diffusivity of 20.5 m^2 s^{-1} is used. Bottom friction is

represented by a quadratic law for the bottom momentum flux with drag coefficient $C_D = 5 \times 10^{-3}$. Vertical turbulence and mixing is calculated through the $k - \epsilon$ configuration of the generic length scale (GLS) turbulence closure (Umlauf and Burchard, 2003) with background vertical eddy viscosity and diffusivity set to 1×10^{-4} m^2 s^{-1} and 1×10^{-5} m^2 s^{-1} respectively. Details on the NEMO implementation of the partial slip lateral boundary condition, quadratic bottom friction law, and GLS turbulence closure scheme are provided by Madec et al. (2012).

At the ocean surface, meteorological conditions and fresh water input from rivers are included. The ocean surface is forced with momentum and heat fluxes from a 33-km global atmospheric reforecasting model suitable for use in ocean modelling (Smith et al., 2014). Forecasts from the period of 2002-2012 are available. Additionally, the inverse barometric effect of the atmospheric pressure is included, an important consideration in storm surge modelling. One simulation employs the western Canada component of the High Resolution Deterministic Prediction System (HRDPS), a nested 2.5 km resolution atmospheric model provided by Environment Canada (Environment Canada, 2014b).

River input provides a significant volume of freshwater to the Salish Sea and can influence stratification, circulation, and primary productivity. However, most rivers in the domain are not gauged so parametrizations were required to represent river flow. Morrison et al. (2011) provides a method for estimating freshwater runoff in the Salish Sea region based on precipitation. Monthly runoff volumes for each watershed for each year from 1970 to 2012 were acquired from Morrison et al. (2011), as well as monthly averages.

Freshwater runoff from each watershed was divided between the rivers in that watershed. The area drained by each river was estimated from Toporama maps by the Atlas of Canada and watershed maps available on the Washington State government website. The watersheds included in our model were Fraser (which represents approximately 44% of the freshwater input into our domain), Skagit (12%), East Vancouver Island (North and South) (12%), Howe (7%), Bute (7%), Puget (6%), Juan de Fuca (5%), Jervis (4%) and Toba (3%). The monthly flow from each river was input as a point source at a depth of 3 metres at the model point closest to the mouth of each river. Incoming water was assumed to be fresh and at surface temperature. A total of 150 rivers were parametrized by this method and their locations are indicated by the blue dots in Figure 1.

Initial conditions for temperature and salinity were taken from a CTD cast in the middle Strait of Georgia taken in Sept 2002 (Pawlowicz et al., 2007). Conditions were initially uniform horizontally and velocity was initialized at zero. The model was spun up for a 15.5 months from the initial conditions above, starting Sept 16, 2002, using atmospheric forcing from 2002-2003, climatological temperature and salinity and sea

surface height at the boundaries, with tides and climatological river output. All storm surge runs were started at least three days prior to the event of interest with zero initial velocities and sea surface height and a stratification profile from model spin up. The modelled sea surface height adjusted to forcing in less than one day.

3   Tidal Evaluation

The model was initially evaluated qualitatively by comparing patterns of tidal amplitude and phase to results from Foreman et al. (1995), focusing on the major M_2 and K_1 constituents. For example, the M_2 amphidrome around Victoria was reproduced as well as the monotonic increase in K_1 amplitude moving northwards along the Strait of Georgia. Once the model was reproducing observed tidal patterns, model results were quantitatively evaluated by comparing modelled harmonic constituents to measured harmonic constituents at tidal measuring stations throughout the domain. Comparisons were made using the complex difference (D), defined as (Foreman et al., 1995):

$$D = [(A_0 \cos g_0 - A_m \cos g_m)^2 + (A_0 \sin g_0 - A_m \sin g_m)^2]^{1/2} \tag{1}$$

where A_0, A_m, g_0 and g_m are the observed and modelled amplitudes and phases. Figure 2 compares modelled and observed amplitude and phase for the M_2 and K_1 tidal constituents for stations along a transect from the Strait of Juan de Fuca through to the Strait of Georgia and Johnstone Strait. Complex differences for these two constituents are also plotted. Comparisons have been made with data from Foreman et al. (1995), Foreman et al. (2004) and Foreman et al. (2012). Station names and numbers are listed in Table 5 in Appendix A.

In general, the K_1 tidal harmonics are well represented by the model with complex differences below 5 cm at all stations except Seymour Narrows (station 27). Seymour Narrows is a very constricted region in Johnstone Strait and is not well resolved by the model. As such, the M_2 amplitude and phase are also poorly reproduced here. The model's M_2 amphidrome, indicated by the drop in amplitude around station 5 (Victoria), is too strong resulting in lower than observed M_2 amplitudes in this region. Additionally, the M_2 phase errors in the Strait of Juan de Fuca (stations 1-7) are quite large, leading to large complex differences in this region. However, the match in the Strait of Georgia (stations 10-24) is very good, with complex differences less than 6 cm, in part due to tidal tuning for highly accurate tides in the main region of interest. Details on the tidal tuning procedure are provided in Appendix A.
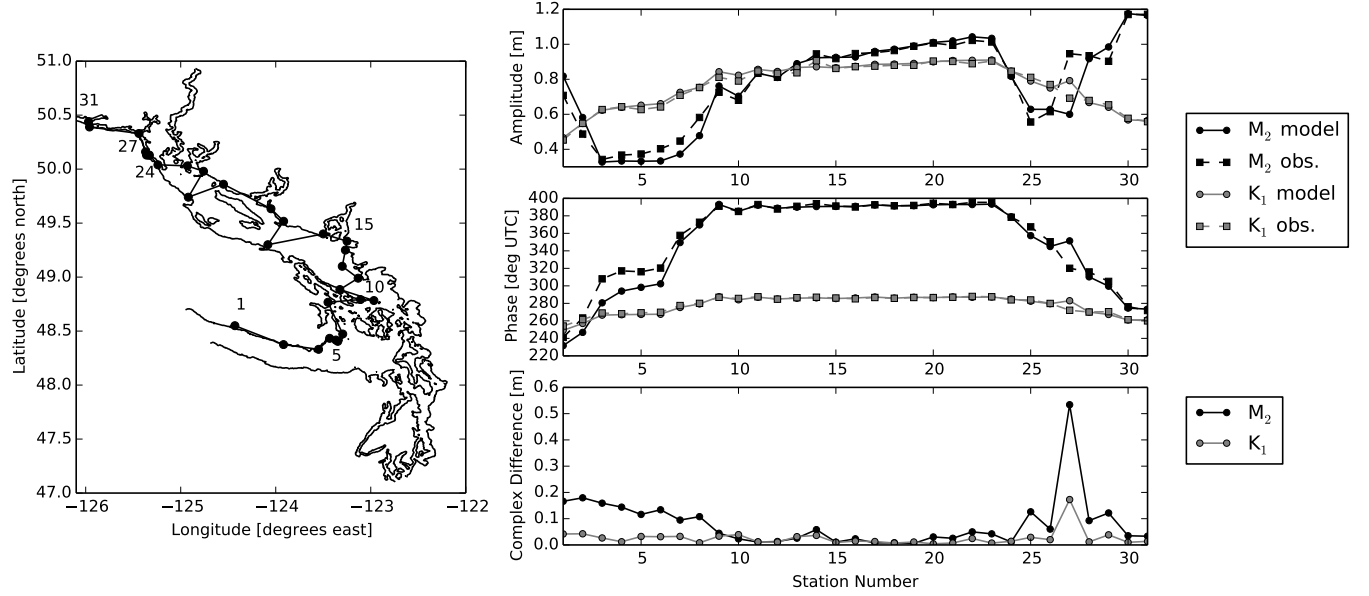
Figure 2: Evaluation of model tidal amplitude and phases for the M_2 and K_1 constituents. On the left, a transect through the stations used for comparison. On the right, modelled M_2 (black) and K_1 (grey) amplitude (top) and phase (middle) compared with observations in the dashed curves of the same colour. The bottom plot displays the M_2 and K_1 complex differences. Station names and numbers are listed Appendix A in Table 5.

4   Storm Surge Hindcasts

A series of storm surge hindcasts is presented next. Storm surge simulations were started from rest at least three days prior to the event of interest to allow for adjustment of model currents. Stratification conditions from model spin-up at a time close to the event (within five days) were chosen to initialize the temperature and salinity fields. Boundary conditions include atmospheric forcing and fresh water input from rivers at the surface, sea surface height anomaly from observations at the open boundary, and tidal forcing with eight tidal constituents. Forcing the model with only eight tidal constituents leads to an error in modelled sea surface height due to the omission of the next leading order tidal constituents such as J_1. Comparisons between full tidal predictions and tidal predictions using eight constituents suggest that this error can approach 40 cm during times of high tidal range, and in particular, during the storm surge season Nov-Feb. As such, storm surge model predictions were corrected by accounting for this error. Additionally, since the sea surface height is calculated about a zero reference level, the modelled water level is determined by adding a long term mean sea level at the specified location to the modelled sea surface height.

Model results have been compared with observations by calculating both the total modelled water level and the modelled residual. The modelled residual is calculated as the difference in model output between

a simulation with all forcing conditions and a simulation forced only with tides and rivers. Water level observations are taken from Fisheries and Oceans Canada (citation?) and are used to calculate the observed residual, defined as the observed water level minus tidal predictions. Tidal predictions are calculated using t_tide (Pawlowicz et al., 2002), a MATLAB tool that calculates tidal harmonics from a given time series, in this case, from the year prior surge event of interest. Additionally, several simulations with varying forcing conditions such as removing atmospheric forcing or removing the sea surface height anomaly at the open boundaries have been completed.

Several significant surge or wind events have been considered in detail, as well as an array of hindcasts to asses model ability in a statistical measure. These cases have been used to assess the model's skill in reproducing water level height and surge amplitude and timing during storm events. The assessment includes comparisons at four permanent tidal measuring stations; Point Atkinson, Victoria, Patricia Bay, and Campbell River (locations indicated in Figure 1). In addition, the contribution to the surge due to several forcing conditions, such as atmospheric forcing and open boundary forcing, has been assessed. We have also examined the spatial variability of the surge as it propagates through the domain and have considered a case with a strong wind event but no significant observed surge. Finally, comparisons between hindcasts using high resolution and low resolution atmospheric forcing have been completed.

The model's skill is reported through a few statistical measures of the the total water level η and the residual δ. First, the mean absolute error ($\bar{e}$), defined as

$$\bar{e} = \text{mean}\left(|M - O|\right), \tag{2}$$

where M and O are the modelled and observed quantities of interest, is a common measure that estimates the average error in the model. Next, a measure comparing the variance of the error to the variance of the observations defined as (Thompson et al., 2003),

$$\gamma^2 = \frac{\text{var}\left(M - O\right)}{\text{var}\left(O\right)}, \tag{3}$$

is also calculated. Smaller values of γ^2 indicate better model skill. This quantity was used by Bernier and Thompson (2006) and Bernier and Thompson (2010) in storm surge predictions in Eastern Canada and is calculated here as a point of comparison. A third measure, called the Willmott skill score (Willmott, 1982), is also used to assess overall model skill in predicting the water level and residual. This quantity is defined

as

$$WS = 1 - \frac{\sum_{i=1}^{N} \left(M_i - O_i\right)^2}{\sum_{i=1}^{N} \left(|M_i'| + |O_i'|\right)^2}, \tag{4}$$

where $M_i' = M_i - \bar{O}$ and $O_i' = O_i - \bar{O}$ and $\bar{O}$ is the mean of the observations. This score is bounded by zero and one. Values close to one indicate good model skill.

4.1 Example Storm Surge Hindcasts

On Feb 4, 2006, a strong storm system with winds over 75 km hr^{-1} coinciding with an unusually high tide led to significant flooding in coastal communities of the Strait of Georgia (Romanowski, 2010). The maximum water level observed at Point Atkinson on this day was 5.46 m, which is 0.82 m higher than the predicted tides, highlighting the significance of this event as it resulted in a large anomaly and also reached water levels close to the highest level ever recorded (5.61 m). A set of hindcast simulations from Feb 1-8, 2006 have been completed.

The model's ability to reproduce this event is demonstrated in Figure 3 which compares observations to corrected model output at Point Atkinson, Victoria, Patricia Bay, and Campbell River. The timing of maximum water level matches well between the observations and the model at all four locations, the most significant contribution to high water being from the tides which are generally well-represented by the model. There is good agreement in the water level maximum at both Victoria and Patricia Bay, with a relative error less than 2%. In fact, there is only a 4.2 cm difference between observed and modelled maximum at Victoria and a 6.9 cm difference at Patricia Bay, the model slightly under predicting in each case. The error at Point Atkinson and Campbell River is slightly more significant, reaching 2.5% and 2.7% respectively, close to 14 cm over predicted at both locations. It is surprising that Victoria and Patricia Bay agree so closely with observations because the M$_2$ tidal amplitudes in the model are known to be too low in this area. When considering the over predicted water levels at Point Atkinson and Campbell River, it is likely that one of the forcing factors is overestimated in this example.

A comparison between observed and modelled residuals is also displayed in the panels on the right. In general, there is a very good agreement between the observed and modelled residuals. The most noticeable difference is a 4-6 hour delay in the model's timing of the maximum residual except at Victoria where the maximum residual is in sync with observations. The errors in maximum residual range from 6.0 cm too high at Victoria to 15.9 cm too low at Campbell River. Both Point Atkinson and Patricia Bay experience a very good match with observed residuals with errors in the maximum less than 2 cm. Note that Point Atkinson
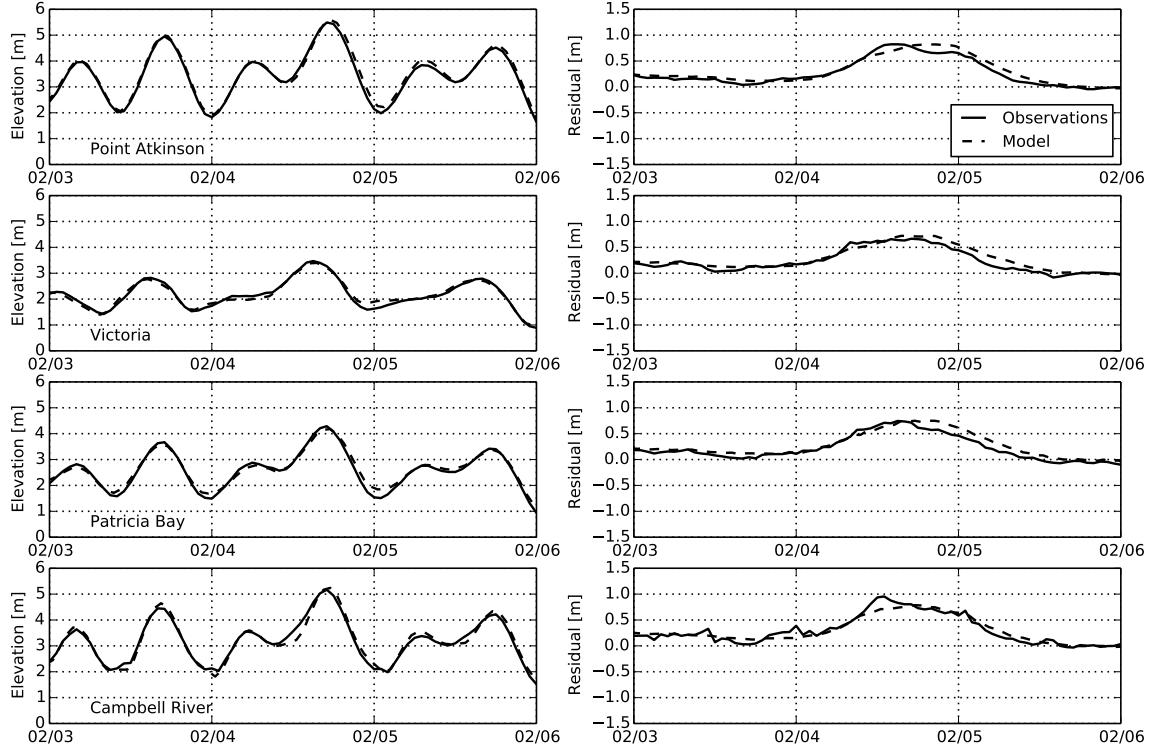
Figure 3: Comparison of observations and model output for the Feb 4, 2006 storm surge. Left: total water level observation (solid) and corrected model (dashed). Right: observed residuals (solid) and modelled residuals (dashed).

and Campbell River realized the largest observed surges at 82 cm and 95 cm respectively. The surges at Victoria and Patricia Bay were observed to be 66 cm and 74 cm.

The maximum water level and maximum residual are important factors in storm surge hindcasts but a better indicator of overall model performance is provided by a group of statistical measures, including the mean absolute error, the observed mean, the modelled mean, γ^2, and the Willmott skill score for both the water level and residuals, in Table 1. The statistics are calculated with hourly output over the three-day period displayed in Figure 3. To begin with, the mean absolute error in the water level ranges from 7.6 cm at Victoria to 13.1 cm at Campbell River, whereas, the mean absolute error in the residuals is smaller at all stations, however, this measure does not account for the large variability in water levels due to the tides. A statistic that does take into account this variability is γ^2 which suggests very good agreement in both the predicted water levels and residuals. Good agreement is also reflected in high Willmott skill scores at all locations. Note that the γ^2 measures and Willmott skill scores degrade slightly for the residuals, likely because the well-tuned tidal signal dominates the water level predictions.

13

	Water Level (η)					Residual (δ)				
Location	$\bar{e}$ (cm)	$\bar{\eta_o}$ (m)	$\bar{\eta_m}$ (m)	γ^2	WS	$\bar{e}$ (cm)	δ_o (m)	δ_m (m)	γ^2	WS
Point Atkinson	10.5	3.46	3.54	0.012	0.996	6.2	0.273	0.309	0.065	0.979
Victoria	7.6	2.18	2.19	0.032	0.992	6.1	0.235	0.278	0.085	0.970
Patricia Bay	9.1	2.60	2.64	0.024	0.992	6.8	0.223	0.278	0.070	0.969
Campbell River	13.1	3.20	3.21	0.041	0.990	5.8	0.303	0.300	0.079	0.978

Table 1: Evaluation of model performance for the Feb 2006 simulation. Mean absolute error ($\bar{e}$), observed mean (subscript o), modelled mean (subscript m), γ^2, and the Willmott skill score (WS) are provided for water level predictions (η) and residuals (δ) during the period displayed in Figure 3 from Feb 3, 2006 to Feb 6, 2006.
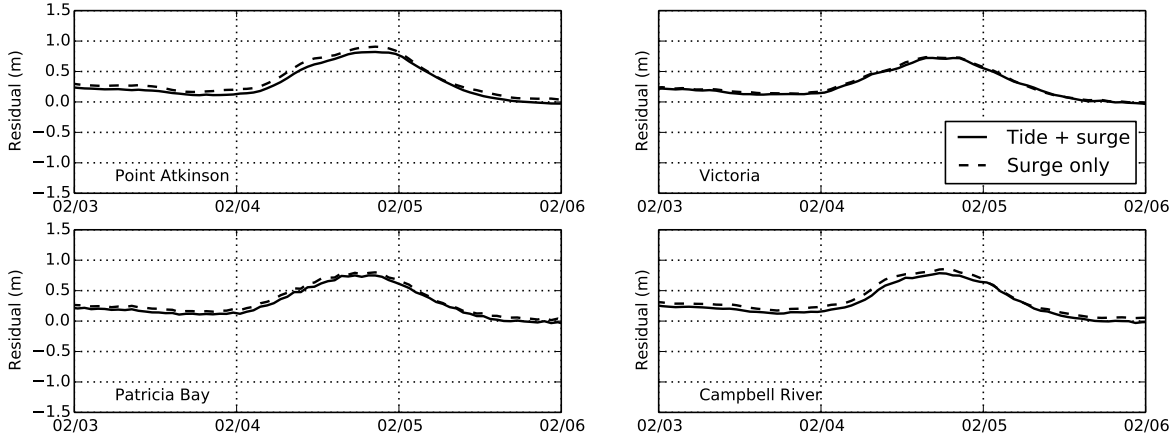

Figure 4: Modelled residuals (solid) compared with a simulation of the surge propagation without tidal forcing (dashed) for the Feb 2006 hindcast.

Next, an assessment of the importance of including the tide-surge interaction, which is important in shallow regions due to nonlinear effects and bottom friction, is presented for this hindcast. A simulation of the surge propagation without including any tidal forcing is compared with the modelled residual in Figure 4. The most significant differences occur at Point Atkinson where the maximum of the surge-only case is 8.7 cm higher than maximum modelled residual, about 10% of the total surge amplitude. In contrast, the tide-surge interaction at Victoria is hardly noticeable. Indeed, a spatial map of the difference between the modelled residual and surge-only difference (not shown here) indicates that the tide-surge interaction is more pronounced after the San Juan and Gulf Islands. The passages between these islands are known for vigorous tidal mixing, which may have a nonlinear effect on the surge propagation. However, the effect is a relatively small overestimate of the surge elevation and no changes to the timing of the surge. So, in operational settings, performing a surge-only simulation and adding the predicted tides *a posteriori* could be more computationally efficient with only a small decrease in the accuracy of the prediction.

An additional storm surge hindcast for Nov 2006 is provided as another means of assessing model perfor-

14

mance and is mentioned briefly here. On Nov 16, 2006 communities in the Strait of Georgia experienced a strong wind storm with speeds upwards of 20 m s^{-1} near Point Atkinson resulting in observed water levels of 5.1 m and a maximum surge amplitude of 83.7 cm. The surge amplitude was lower at the other stations, reaching no more than 68 cm. The model performs reasonably well in this hindcast; Willmott skill scores are greater than 0.94 as outlined in Table 2. The best match in maximum surge occurred at Campbell River with a 6.2 cm underestimate by the model. The timing of the maximum surge at Campbell River was identical with observations and too early at the other the stations.

Location	Water Level (η)					Residual (δ)				
	$\bar{e}$ (cm)	$\bar{\eta_o}$ (m)	$\bar{\eta_m}$ (m)	γ^2	WS	$\bar{e}$ (cm)	δ_o (m)	δ_m (m)	γ^2	WS
Point Atkinson	9.8	3.42	3.43	0.034	0.991	7.7	0.290	0.247	0.128	0.950
Victoria	9.1	2.16	2.11	0.070	0.978	6.2	0.222	0.202	0.171	0.946
Patricia Bay	10.0	2.57	2.53	0.049	0.985	6.6	0.235	0.203	0.144	0.947
Campbell River	10.7	3.20	3.26	0.037	0.989	6.2	0.254	0.236	0.140	0.952

Table 2: Evaluation of model performance for the Nov 2006 hindcast. Statistics were calculated over the period Nov 14, 2006 to Nov 17, 2006.

4.2 Factors Contributing to Storm Surges

Next, an assessment of the factors that are most important in scenarios leading up to storm surges is presented for the Feb 2006 storm surge in Figure 5. The modelled residual from four simulations have been plotted. First, a simulation with all the forcing conditions, including tides, atmospheric forcing, rivers, and sea surface height anomaly, is shown in the dashed black curve. Next, a simulation with all forcing except the atmospheric forcing is presented in solid grey and a simulation with all forcing except the sea surface height anomaly is shown solid black. Finally, a simulation with only wind forcing, that is no anomaly and no inverse barometer effect due to pressure, is shown in the dashed grey curve. It is clear that the sea surface height anomaly contributes most significantly to the surge at each of these locations. When the sea surface height anomaly is not included as a forcing condition, the surge drops from a maximum 82 cm to 11 cm at Point Atkinson and its maximum occurs eight hours later. A similar drop in the maximum surge and delay in timing of the maximum surge is observed at the other locations. The atmospheric model indicates southeasterly winds near Point Atkinson during the onset of the surge but after the peak surge has passed the winds shift to westerly. A strong westerly wind would cause an elevated sea surface height at Point Atkinson as water piles against the coast, explaining the delay in peak surge when only atmospheric forcing is used since the winds shift to westerly after the peak surge has passed. A simulation with only wind forcing produces a surge of 7.8 cm at Point Atkinson, a small fraction of the total observed surge, and

only centimetres at the other locations. Note that this wind-induced surge occurs well after the peak surge occurred in both the observations and simulations with full forcing.

The contribution to the surge due to atmospheric forcing appears to be geographically dependent, its removal leading to a drop of about 2.5 cm in the maximum surge at Point Atkinson and 2.3 cm at Campbell River. Interestingly, the surge amplitude increases by 4.8 cm at Victoria and 3.6 cm at Patricia Bay when atmospheric forces are neglected. The southeasterly winds over the Strait of Georgia could be acting to push water away from the southern tip of Vancouver Island, resulting in a slight decrease in the surge amplitude at Victoria and Patricia Bay when wind effects are included in the model. Additionally, the surge amplitude decreases by a few centimetres if the inverse barometer effect due to atmospheric pressure is not included.

These comparisons point to the importance of including, as a forcing condition at the open boundary, the surge entering the domain from the Pacific Ocean. Storms travelling over the Pacific Ocean towards the west coast of the northern United States and Canada can induce elevated sea levels along the coastline which then enter the Salish Sea system through the Strait of Juan de Fuca. In a model domain that does not include the Pacific Ocean, this effect must be included as a boundary condition. Previous simulations by Murty et al. (1995) suggest that the inverse barometer effect and the surge entering the system through the Strait of Juan de Fuca contribute most significantly to storm surges in this domain. A detailed assessment of the effect of the local atmospheric conditions and winds should be performed with high resolution atmospheric forcing data.

4.3   Spatial Extent of Surge

On Dec 15, 2006, a major storm with wind gusts over 120 km hr^{-1} caused significant damage to many coastal communities on the Pacific Northwest. Although the storm was very strong and the observed residual at Point Atkinson reached 84 cm, this event did not coincide with high tide and so no significant or reported flooding occurred in the Vancouver area (Forseth, 2012). This event has been used to examine the propagation of the surge throughout the domain and spatial variations in the surge amplitude. First, an assessment of the accuracy of the hindcast is provided.

Point Atkinson observed a maximum surge amplitude of 84 cm, which is approximately 28 cm higher than the modelled residual, however the timing of the surge agrees almost exactly as displayed in Figure 6. The best agreement occurs at Victoria where the observed surge was 62 cm and the model returned 44 cm. At all of the locations, the model predicted the maximum surge to occur within 3 hours of the observed surge. Typically, the modelled surge was too early, in contrast to the later predictions in the Feb 4, 2006
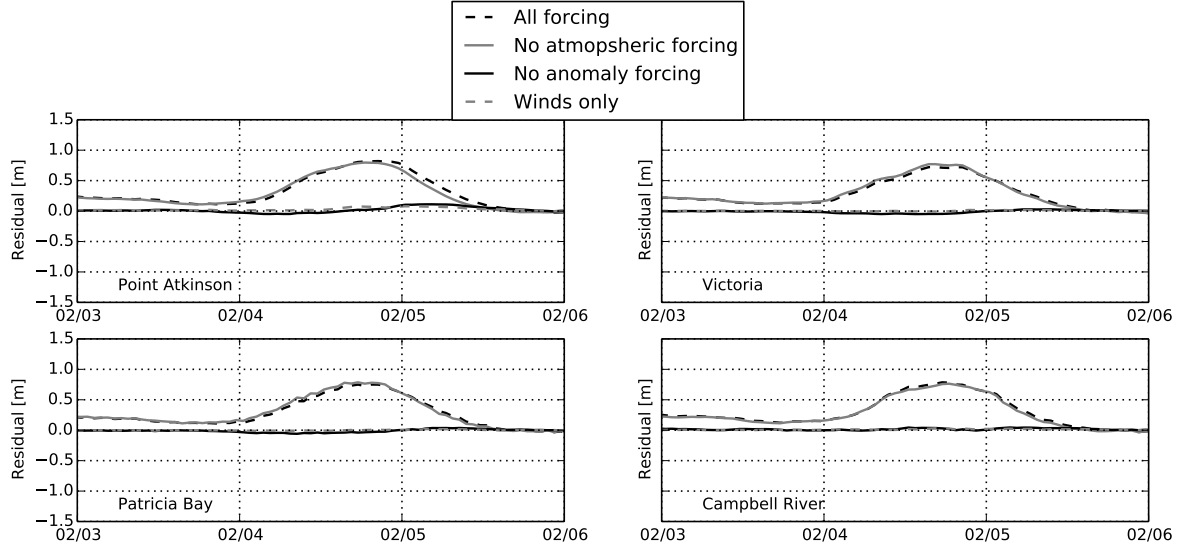
Figure 5: Comparison of the modelled residual for four simulations in Feb 2006: A simulation with all forcing (solid black), a simulation without atmospheric forcing (solid grey), a simulation without the sea surface height anomaly (dashed black), and a simulation with only wind forcing, i.e. no sea surface height anomaly or pressure (dashed grey).

case. Error and skill scores for the modelled water level and the modelled residual are provided in Table 3. All Willmott skill scores rank above 0.89 and the γ^2 measure also indicates good agreement between model and observations. The modelled residuals are on average too low and have a lower skill score than the Feb 2006 case. This could be due to a number of factors. First, the very large wind speeds observed during this storm are significantly underrepresented by the atmospheric model leading to lower wind stress and less piling of water against the coast. Second, the anomaly forcing at the open boundaries could be too low. The observed residual at Tofino, BC (a point near by but outside of the domain) is up to 10 cm lower than the observed residual at Neah Bay, WA (a point near by but inside of the domain). Since the storm surge is less sensitive to wind forcing at the surface than anomaly forcing at the open boundaries, the latter is likely the case.

Location	Water Level (η)					Residual (δ)				
	$\bar{e}$ (cm)	$\bar{\eta}_o$ (m)	$\bar{\eta}_m$ (m)	γ^2	WS	$\bar{e}$ (cm)	δ_o (m)	δ_m (m)	γ^2	WS
Point Atkinson	10.5	3.45	3.47	0.025	0.994	11.1	0.212	0.186	0.275	0.891
Victoria	9.6	2.23	2.16	0.042	0.984	7.9	0.190	0.156	0.223	0.911
Patricia Bay	9.2	2.63	2.58	0.031	0.990	9.5	0.193	0.149	0.260	0.889
Campbell River	10.6	3.23	3.28	0.030	0.992	9.4	0.191	0.163	0.247	0.905

Table 3: Evaluation of model performance for the Dec 2006 hindcast. Statistics were calculated over the period Dec 14, 2006 to Dec 17, 2006.
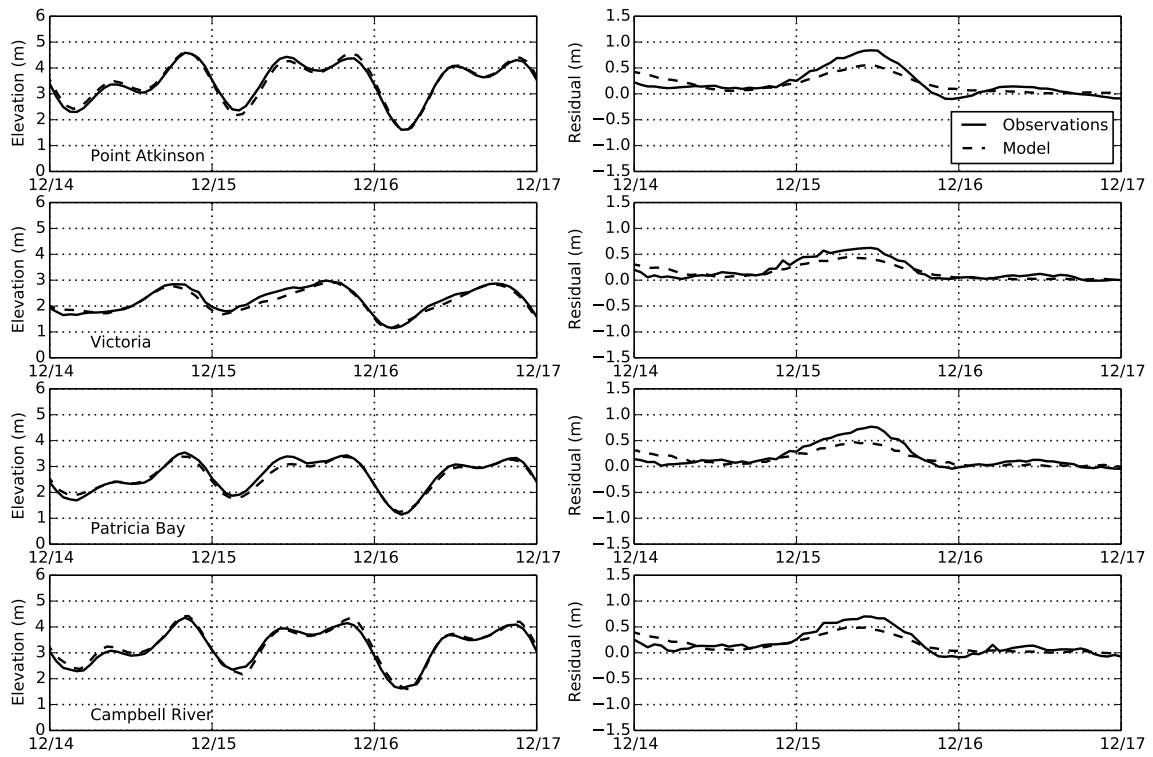
17

Figure 6: Comparison of observed and modelled water level and residuals during the Dec 15, 2006 storm surge simulation.
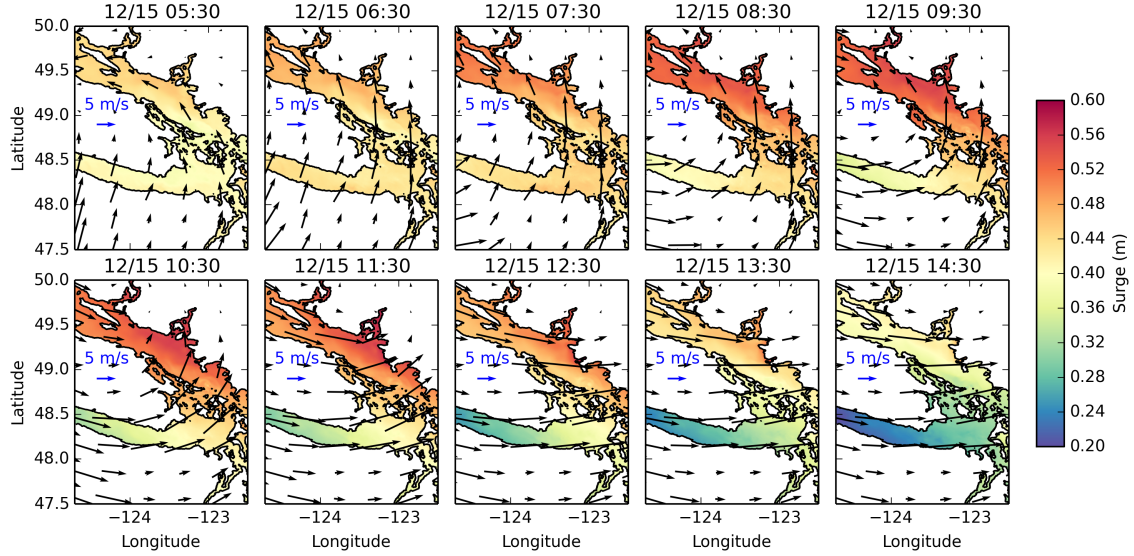
Figure 7: Propagation of the storm surge on Dec 15, 2006. Modelled residual every hour starting on Dec 15 at 05:30 UTC. Time advances from top left to bottom right. Wind vectors from the atmospheric forcing are overlaid in black.

The evolution and spatial distribution of the surge is highlighted in Figure 7 where the modelled residual is plotted every hour beginning on Dec 15 at 05:30 UTC through to Dec 15 at 14:30 UTC. The surge enters the system from the Strait of Juan de Fuca, peaking between Dec 15 at 9:30 UTC and Dec 15 at 11:30 UTC and then begins to subside throughout the entire domain. Notably, the Strait of Georgia experiences the largest surge values, upwards of 60 cm, whereas the Juan de Fuca region experiences a maximum surge around 45 cm. Additionally, the coastal areas on the mainland side of the Strait of Georgia experience slightly higher surges (∼10 cm) than the Vancouver Island side, likely due to the southerly wind in the atmospheric model pushing water against the mainland coast. At about 11:30 UTC, the winds at Point Atkinson switch to northwesterly and then westerly, further amplifying the surge along the mainland coast.

An evaluation of the spatial distribution of the surge in a simulation without atmospheric forcing is provided in Figure 8. In this case, the surge amplitude across the Strait of Georgia is uniform with no pronounced difference between the mainland side and Vancouver Island side. While the surge entering the domain from the Pacific Ocean is the leading order contribution, the winds may induce localized changes to the surge amplitude. Interestingly, the winds over the Strait of Juan de Fuca cause a decrease in surge amplitude in this region as the winds are acting to push the water towards the mainland. Even without atmospheric forcing, there is still a significant difference in surge amplitude between the Strait of Georgia and the Strait of Juan de Fuca, perhaps because the Strait of Georgia is also affected by the surge entering
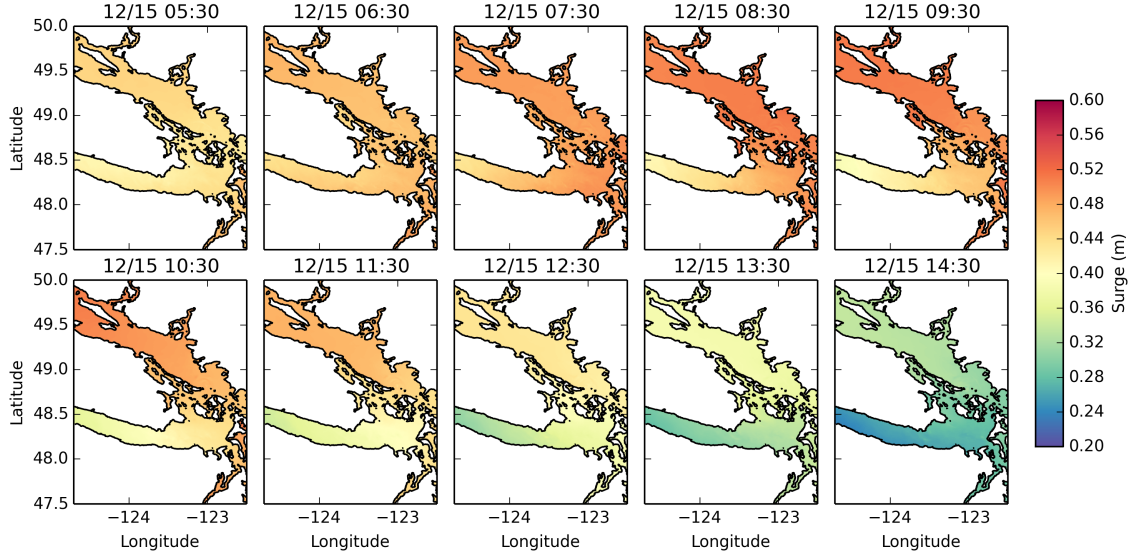
19

Figure 8: As in Figure 7 but for a simulation that does not include atmospheric forcing.

the domain from Johnstone Strait at the northern boundary or the incoming surge wave is partially reflected from the mainland coast.

4.4 Strong Wind Event

Next, a relatively strong wind event recorded at Point Atkinson on Nov 19, 2009 is considered. As recorded in the Environment Canada Climate Data archives (Environment Canada, 2014a), the maximum hourly wind speed at Point Atkinson was 18.6 m s^{-1} and the largest gust observed was 25.8 m s^{-1} or 93 km hr^{-1}. In addition, large wind speeds over 15 m s^{-1} persisted for over 9 hours. Yet, the surge associated with this event is rather small when compared to the previous two cases as shown in Figure 9 where we have plotted the wind speed at Point Atkinson, sea surface height anomaly forcing at the open boundaries, and observed and modelled residuals at Point Atkinson. Two significant surge events are noted, the first occurring on Nov 19 with an observed amplitude of about 50 cm at Point Atkinson, and a second, larger surge of 62.5 cm on Nov 20. Surprisingly, the strong wind event of Nov 19 was associated with the smaller of the two surges. Neither of the surges occurred during a high tide and so no high water level events were recorded. Although not shown here, the other three locations also observed a maximum surge on Nov 20, which appears to be linked to a secondary high wind event and another surge entering the system at Tofino and Port Hardy.

Danard et al. (2003) discuss the role of wind fetch, the distance over which wind acts on the surface of a water basin, in setting up seiche motion in lakes and its contribution to storm surges. As wind blows over
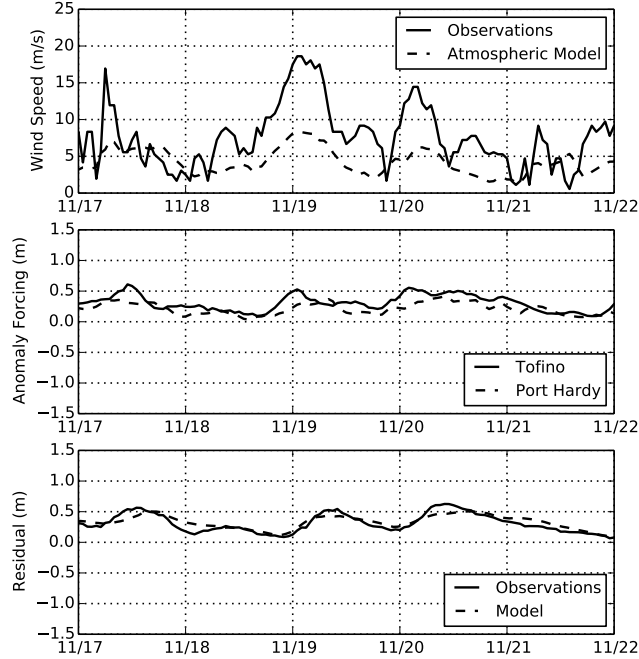
Figure 9: Wind and storm surge conditions at Point Atkinson for a strong wind event on Nov 19, 2009. Top: Wind speed from Environment Canada observations (Environment Canada, 2014a) at Point Atkinson (solid) and from the atmospheric model (CGRF) at a grid point near Point Atkinson (dashed). Middle: Sea surface height anomaly at Tofino (solid) and Port Hardy (dashed) used as forcing conditions at the western and northern open boundaries. Bottom: Observed (solid) and modelled (dashed) residuals at Point Atkinson.

the surface of a lake, the water level becomes elevated on the downwind side and depressed on the upwind side in response to the wind-induced currents. The longer the fetch, the more significant the tilting of the water surface. These changes in water level can also contribute to storm surges. During the high wind events on Nov 19 and Nov 20, the winds at Point Atkinson were directed to the west, explaining the lack of strong surge observed during this event since wind stresses would act to depress the water on the east side of the basin. In fact, the surge amplitude at Victoria on Nov 20 was 64.7 cm which is slightly higher than that observed at Point Atkinson (62.5 cm). Of the cases considered so far, this is the only example where the surge amplitude at Victoria was higher than that at Point Atkinson. This event observed a higher surge at Victoria than the Dec 2006 event, further highlighting the role that winds plays in setting up local variations in the surge. In this case, the model results do not reflect a higher surge at Victoria (46.1 cm versus 50.5 cm at Point Atkinson), perhaps due to an underestimate in the wind speed and some discrepancies in the wind direction of the atmospheric forcing.

Once again, an evaluation of the model skill for this hindcast is provided in Table 4. The modelled water levels and residuals are too high, except at Victoria. Although Victoria has the smallest mean error in both

the water level and residuals, its Willmott skill score and γ^2 values rank low when compared to the other stations. Generally, the skills scores are very good, scoring above 0.89 at all stations.

Location	Water Level (η)					Residual (δ)				
	$\bar{e}$ (cm)	$\bar{\eta_o}$ (m)	$\bar{\eta_m}$ (m)	γ^2	WS	$\bar{e}$ (cm)	δ_o (m)	δ_m (m)	γ^2	WS
Point Atkinson	14.0	3.44	3.55	0.012	0.995	6.1	0.313	0.331	0.237	0.914
Victoria	9.9	2.26	2.24	0.023	0.994	4.8	0.323	0.293	0.245	0.899
Patricia Bay	11.2	2.60	2.65	0.020	0.993	6.0	0.277	0.290	0.272	0.901
Campbell River	13.5	3.22	3.27	0.019	0.995	4.9	0.326	0.314	0.217	0.924

Table 4: Evaluation of model performance for the Nov 2009 hindcast. Statistics were generated over the period Nov 17, 2009 to Nov 22, 2009.

4.5   High Resolution Atmospheric Forcing

The above comparison between the modelled and observed winds at Point Atkinson suggests that the atmospheric forcing product (CGRF) may not be adequate to produce accurate storm surge hindcasts since the wind speeds are substantially lower than observed. CGRF is a global atmospheric reforecasting model with horizontal resolution approximately 33 km over the Salish Sea domain, which is problematic since the Strait of Georgia itself is only about 30 km wide. As such, there are only one or two grid cells that are entirely over water in our domain, resulting in overly damped wind speeds at grid points close to land such as Point Atkinson. To determine the effect of under-resolved wind forcing on the storm surge hindcasts we compare simulations that have been forced with 1) the low resolution CGRF model and 2) a high resolution (2.5 km) HRDPS model from Environment Canada. These simulations are performed for a storm surge that occurred on Dec 17, 2012 and cover the time period Dec 14-19, 2012. The high resolution product is not available for the hindcasts already discussed.

First, a comparison of the wind speed and direction for the two models and observations is provided in Figure 10 at Point Atkinson and at Sandheads, a lighthouse station in the southern Strait of Georgia. For each of the models, the wind speed and direction at the closest grid point to the longitude/latitude of Point Atkinson and Sandheads is used for comparison. Although the low resolution CGRF model has a grid spacing of 33 km, two grid points align closely with these locations. At Point Atkinson, the high resolution model is in very good agreement with observations for both the wind speed and direction, however, the low resolution CGRF model significantly underestimates the wind speed during high wind periods on Dec 15, 2012 and Dec 17, 2012. At Sandheads, both the low resolution and high resolution models have good agreement with observations. The low resolution model has a very good match at Sandheads likely because this grid cell happens to be mostly over water. Although not shown here, both models have a similar sea
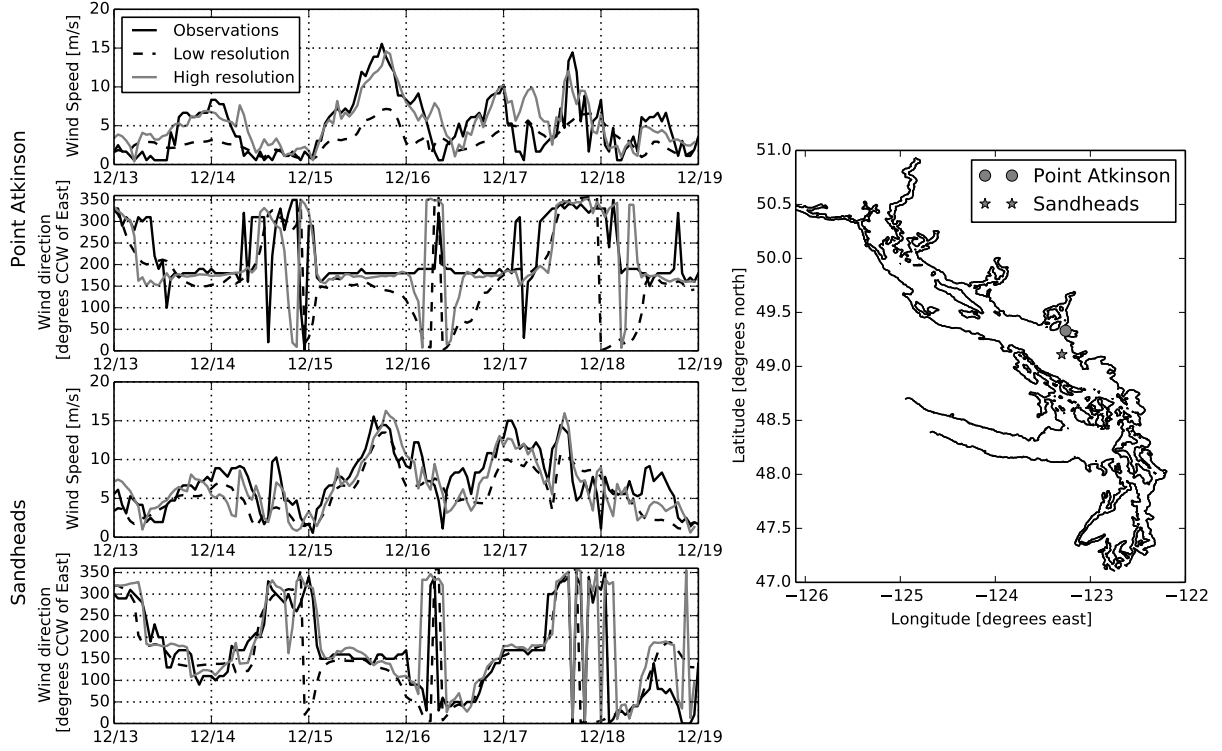
Figure 10: Comparison of observed and modelled winds during Dec 2012 storm surge simulation at Point Atkinson (upper) and Sandheads (lower). Observed winds shown in solid black, low resolution CGRF model in dashed black and high resolution model in grey. Observations are from the Environment Canada Climate Data archives (Environment Canada, 2014a).

level atmospheric pressure at these two locations.

Modelled and observed residuals for this simulation are displayed in Figure 11 where it is apparent that both of the simulations agree well with the observations. Willmott skill scores for both modelled residuals are above 0.92 at these four locations. Further, the modelled residuals deviate only slightly from each other, most noticeable at Point Atkinson during the large wind event on Dec 15, 2012 where simulation with the low resolution atmospheric forcing has a residual that is 5 cm higher. Although the wind speeds on Dec 15, 2012 are quite high, this event did not result in any flooding or residuals greater than 50 cm. Significant flooding occurred later, on Dec 17, 2012, where the observed surge amplitude at Point Atkinson was 68.3 cm. Even though the low resolution model significantly underpredicts the wind speed at some locations, it performs comparable to forcing with high resolution products. This result further demonstrates that the local wind is not the most important factor for setting up storm surges over this domain.
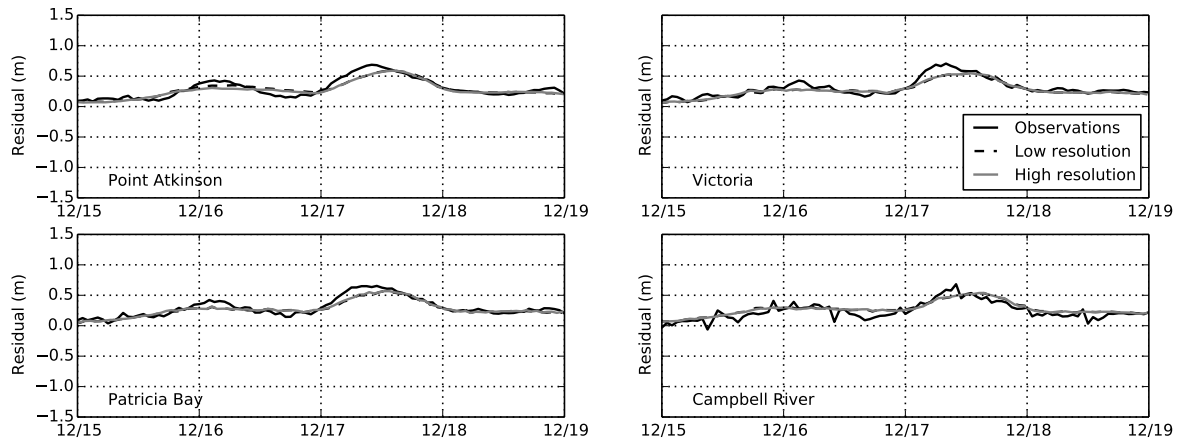
Figure 11: Comparison of observed (solid black) and modelled residuals for the Dec 2012 storm surge simulation. Modelled residuals from two simulations using a low resolution (dashed) and high resolution (grey) atmospheric products are shown.

5 Discussion

In this article, we have configured a three-dimensional numerical ocean model of the Salish Sea for accurate hindcasts of storm surges in the Strait of Georgia. The model is forced with eight tidal constituents at the western and northern open boundaries, as well as sea surface height anomaly from de-tided observations at Tofino and Port Hardy. Additionally, wind stress and an inverse barometer effect were forced at the ocean surface using an atmospheric reforecasting product called CGRF (Smith et al., 2014). Storm surge simulations began with zero initial conditions for the currents and sea surface height and were commenced several days prior to the event of interest to spin up the velocity fields.

Hindcasts of five significant events in February 2006, November 2006, December, November 2009, and December 2012 were simulated. In general, the model performs well at reproducing the observed water level heights and residuals, with Willmott skill scores greater than 0.88 in all cases. We have also assessed the relative importance of different forcing factors contributing to the storm surge. The sea surface height anomaly entering the system from the Pacific Ocean contributes most significantly to the surge amplitude, in agreement with previous studies in this region (Murty et al., 1995). Although the large scale wind patterns and atmospheric conditions are important in setting up the surge on the Pacific Ocean boundaries, the local winds within the Strait of Georgia are not the leading order contribution to surge amplitude. However, the local wind patterns can set up small spatial differences in the surge, resulting in higher surges on the mainland side of the Strait of Georgia due to the usually southerly winds during storm surge season. Additionally, surge amplitudes in the Strait of Georgia are typically higher than those in the Strait of Juan de Fuca,

perhaps due to anomalies entering from both the northern and southern regions or a partial reflection from the mainland coast. Results from an additional simulation with no tidal forcing but only surge propagation and atmospheric forcing found that nonlinear effects due to the tide-surge interaction were most important north the San Juan and Gulf Islands. The modelled surge amplitude increased by about 10% at Point Atkinson when the tide-surge interaction was neglected in one example.

Comparisons between high resolution and low resolution atmospheric forcing further suggest that the local winds are not the leading order factor in setting up large surge amplitudes. The low resolution model significantly underestimated wind speeds in certain areas of the domain, however, it performed just as accurately in reproducing surge amplitudes as the high resolution product. Although the high resolution model delivers fine scale detail and more accurate local wind patterns, it did not provide any improvement to the surge hindcast. Since both of these products provide the same level of accuracy for storm surge hindcasts, in the future we will use the high resolution atmospheric model to produce real-time storm surge predictions, even though most of out testing was performed with the low resolution model.

Several factors considered in other storm surge modelling studies have been neglected in these simulations. Primarily, effects due to wetting and drying have not been included. This is an important factor to consider in shallow, low lying areas where water levels retreat significantly to reveal land. In this article, the four locations used to assess storm surge accuracy are not in shallow regions and so wetting and drying is not considered to be important. However, several communities in the Strait of Georgia, such as Boundary Bay and Crescent Beach, are in shallow regions and are typically most affected by storm surge during the winter season. As such, efforts to include wetting and drying will be considered in the future. Additionally, the sea surface height anomaly from Neah Bay, forecasted by the National Oceanic and Atmospheric Administration (NOAA), will be used in future real-time water level predictions during the storm surge season. Lastly, flooding effects due to wave run up is left for a more detailed inundation study with higher resolution in the near-shore areas.

Since the Strait of Georgia is a large, semi-enclosed body of water storm surges can behave and evolve differently than in other coastal regions. For instance, the complicated coastlines and local wind patterns result in important spatial variations in the surge amplitude. As such, the strong wind caused by a large storm is not the only factor to be considered in community preparedness for surge conditions. The geometry of the Strait and local wind patterns render communities on the mainland side of the southern Strait of Georgia more susceptible to surges. Additionally, communities such as Campbell River are at risk due to the long fetch and predominately southerly winds during the winter months.

Finally, difficulties in reproducing accurate M_2 tidal harmonics in both the Strait of Georgia and the Strait of Juan de Fuca have been highlighted in this study among others (Stronach et al., 1993; Foreman et al., 2004). Future work will attempt to improve model accuracy by examining mixing parametrizations and energy dissipation due to bottom friction and their effect on tidal harmonics. Additionally, a biological-chemical modelling component will be added.

A   Appendix

This section details the procedure used to tune the tidal forcing for a good match with observations in the Strait of Georgia. Originally, the eight most important tidal elevation and currents harmonics were extracted from a tide prediction tool called Webtide (Foreman et al., 2000) at the western Juan de Fuca boundary. At the northern boundary, M_2 and K_1 tidal harmonics for both elevation and currents were taken from Thomson and Huggett (1980), as well as elevation harmonics for O_1 and S_2. The remaining constituents were extrapolated from Webtide based on the ratio between M_2/S_2 amplitudes and phase differences for the semi-diurnal constituents and K_1/O_1 for the diurnal constituents. However, these forcing conditions did not result in a good match between observed and modelled tidal elevation harmonics in the Strait of Georgia, the main region of interest (although the matches in the Strait of Juan de Fuca were adequate). As such, tidal forcing was tuned, by first adjusting the western boundary M_2 and K_1 phase and K_1 amplitude for a good match in the Strait of Georgia (specifically at Point Atkinson, Gibsons Landing, Winchelsea and Halfmoon Bay). This tuning was performed on simulations that used only M_2 and K_1 forcing. Next, the M_2 and K_1 fluxes at the northern boundary were adjusted because the cross-sectional area of transect used by Thomson and Huggett (1980) to measure tidal currents in Johnstone Strait is smaller than the cross-sectional area of our northern boundary. Finally, the remaining constituents were added, starting with O_1, then S_2, and then in pairs P_1/N_2 and Q_1/K_2. Adjustments were made if the addition of new constituents hindered performance of the main M_2 and K_1 components.

Below, Table 5 compares the M_2 and K_1 elevation harmonics with data from Foreman et al. (1995), Foreman et al. (2004) and Foreman et al. (2012). Overall, the average complex difference for M_2 is 8.05 cm and for K_1 is 2.58 cm, but both constituents perform very well in the Strait of Georgia region.

B   Acknowledgements

References

Abeysirigunawardena, D. S., D. J. Smith, and B. Taylor (2011). Extreme sea surge responses to climate variability in coastal British Columbia, Canada. *Annals of the Association of American Geographers 101*(5), 992–1010.

Bernier, N. and K. Thompson (2006). Predicting the frequency of storm surges and extreme sea levels in the northwest Atlantic. *Journal of Geophysical Research: Oceans (1978–2012) 111*, C10009.

Bernier, N. and K. Thompson (2007). Tide-surge interaction off the east coast of Canada and northeastern United States. *Journal of Geophysical Research: Oceans (1978–2012) 112*, C06008.

Bernier, N. and K. Thompson (2010). Tide and surge energy budgets for Eastern Canadian and Northeast US waters. *Continental Shelf Research 30*(3), 353–364.

Bobanović, J., K. R. Thompson, S. Desjardins, and H. Ritchie (2006). Forecasting storm surges along the east coast of Canada and the North-Eastern United States: The storm of 21 January 2000. *Atmosphere-Ocean 44*(2), 151–161.

Crean, P., T. S. Murty, and J. Stronach (1988a). *Mathematical modelling of tides and estuarine circulation: The coastal seas of southern British Columbia and Washington state*, Volume 30. American Geophysical Union.

Crean, P. B., T. S. Murty, and J. A. Stronach (1988b). Numerical-simulation of oceanographic processes in the waters between Vancouver Island and the mainland. *Oceanography and Marine Biology 26*, 11–142.

Danard, M., A. Munro, and T. Murty (2003). Storm surge hazard in Canada. *Natural Hazards 28*(2-3), 407–434.

Engedahl, H. (1995). Use of the flow relaxation scheme in a three-dimensional baroclinic ocean model with realistic topography. *Tellus A 47*(3), 365–382.

Environment Canada (2014a). Climate Database. http://climate.weather.gc.ca/index_e.html.

Environment Canada (2014b). High Resolution Deterministic Prediction System. https://weather.gc.ca/grib/grib2_HRDPS_HR_e.html.

Flather, R. A. (1994). A storm surge prediction model for the northern Bay of Bengal with application to the cyclone disaster in April 1991. *Journal of Physical Oceanography 24*(1), 172–190.

Foreman, M., W. Crawford, J. Cherniawsky, R. Henry, and M. Tarbotto (2000). A high-resolution assimilating tidal model for the northeast Pacific Ocean. *Journal of Geophysical Research 105*(C1), 28,629–28,652.

Foreman, M., D. Stucchi, K. Garver, D. Tuele, J. Isaac, T. Grime, M. Guo, and J. Morrison (2012). A circulation model for the Discovery Islands, British Columbia. *Atmosphere-Ocean 50*(3), 301–316.

Foreman, M., G. Sutherland, and P. Cummins (2004). M_2 tidal dissipation around Vancouver Island: an inverse approach. *Continental shelf research 24*(18), 2167–2185.

Foreman, M. G. G., R. A. Walters, R. F. Henry, C. P. Keller, and A. G. Dolling (1995). A tidal model for eastern Juan de Fuca Strait and the southern Strait OF Georgia. *Journal of Geophysical Research-Oceans 100*(C1), 721–740.

Forseth, P. (2012). Adaptation to sea level rise in metro Vancouver: A review of literature for historical sea level flooding and projected sea level rise in metro Vancouver. Technical report, Simon Fraser University.

Giddings, S., P. MacCready, B. Hickey, N. Banas, K. Davis, S. Siedlecki, V. Trainer, R. Kudela, N. Pelland, and T. Connolly (2014). Hindcasts of potential harmful algal bloom transport pathways on the Pacific Northwest coast. *Journal of Geophysical Research: Oceans 119*(4), 2439–2461.

Gray, M., M. Danard, R. Flather, F. Henry, T. Murty, S. Venkatesh, and C. Jarvis (1984). A preliminary investigation using a Nova Scotia storm surge prediction model. *Atmosphere-Ocean 22*(2), 207–225.

Haugerud, R. A. (1999). *Digital elevation model (DEM) of Cascadia, latitude 39N-53N, longitude 116W-133W*. U. S. Geological Survey Open-File Report 99-369. http://pubs.usgs.gov/of/1999/0369/.

Hubbert, G. D. and K. L. McInnes (1999). A storm surge inundation model for coastal planning and impact studies. *Journal of Coastal Research 15*(1), 168–185.

Lane, E. M. and R. A. Walters (2009). Verification of RICOM for storm surge forecasting. *Marine Geodesy 32*(2), 118–132.

Madec, G. et al. (2012). NEMO ocean engine, Note du Pole de modèlisation. France. Ver 3.4, ISSN No 1288-1619.

Marinone, S. G., S. Pond, and J. Fyfe (1996). A three-dimensional model of tide and wind-induced residual currents in the central Strait of Georgia, Canada. *Estuarine Coastal and Shelf Science 43*(2), 157–182.

Masson, D. and P. F. Cummins (2004). Observations and modeling of seasonal variability in the Straits of Georgia and Juan de Fuca. *Journal of Marine Research 62*(4), 491–516.

Masson, D. and I. Fine (2012). Modeling seasonal to interannual ocean variability of coastal British Columbia. *Journal of Geophysical Research 117*, C10019.

Morrison, J., M. Foreman, and D. Masson (2011). A method for estimating monthly freshwater discharge affecting British Columbia coastal waters. *Atmosphere-Ocean 50*(1), 1–8.

Murty, T., S. Venkatesh, M. Danard, and M. El-Sabh (1995). Storm surges in Canadian waters. *Atmosphere-Ocean 33*(2), 359–387.

Pawlowicz, R., B. Beardsley, and S. Lentz (2002). Classical tidal harmonic analysis including error estimates in MATLAB using T_TIDE. *Computers & Geosciences 28*(8), 929–937.

Pawlowicz, R., O. Riche, and M. Halverson (2007). The circulation and residence time of the Strait of Georgia using a simple mixing-box approach. *Atmos. Ocean 45*, 173–193.

Romanowski, S. A. (2010). Storm surge flooding: Risk perception and coping strategies of residents in Tsawwassen, British Columbia. Master's thesis, University of Alberta.

Smith, G. C., F. Roy, P. Mann, F. Dupont, B. Brasnett, J.-F. Lemieux, S. Laroche, and S. Bélair (2014). A new atmospheric dataset for forcing ice–ocean models: Evaluation of reforecasts using the Canadian global deterministic prediction system. *Quarterly Journal of the Royal Meteorological Society 140*(680), 881–894.

Stronach, J., J. Backhaus, T. Murty, et al. (1993). An update on the numerical simulation of oceanographic processes in the waters between Vancouver Island and the mainland: the GF8 model. *Oceanography and Marine Biology: An annual review 31*, 1–86.

Sutherland, D. A., P. MacCready, N. S. Banas, and L. F. Smedstad (2011). A model study of the Salish Sea estuarine circulation. *Journal of Physical Oceanography 41*(6), 1125–1143.

Thompson, K. R., J. Sheng, P. C. Smith, and L. Cong (2003). Prediction of surface currents and drifter trajectories on the inner Scotian Shelf. *Journal of Geophysical Research: Oceans (1978–2012) 108*(C9), 3287.

Thomson, R. E. (1981). *Oceanography of the British Columbia coast*, Volume 56. Department of Fisheries and Oceans Sidney, BC.

Thomson, R. E. and W. S. Huggett (1980). M_2 baroclinic tides in Johnstone Strait, British Columbia. *Journal of Physical Oceanography 10*, 1509–1539.

Umlauf, L. and H. Burchard (2003). A generic length-scale equation for geophysical turbulence models. *Journal of Marine Research 61*(2), 235–265.

Weisberg, R. H. and L. Zheng (2006). Hurricane storm surge simulations for Tampa Bay. *Estuaries and Coasts 29*(6), 899–913.

Willmott, C. J. (1982). Some comments on the evaluation of model performance. *Bulletin of the American Meteorological Society 63*(11), 1309–1313.

Xu, H., K. Zhang, J. Shen, and Y. Li (2010). Storm surge simulation along the US East and Gulf Coasts using a multi-scale numerical model approach. *Ocean dynamics 60*(6), 1597–1619.

Yang, Z. and T. Khangaonkar (2010). Multi-scale modeling of Puget Sound using an unstructured-grid coastal ocean model: from tide flats to estuaries and coastal waters. *Ocean Dynamics 60*(6), 1621–1637.

	Station name	Longitude	Latitude	M$_2$			K$_1$		
				R	$\Delta\phi$ (deg)	D (cm)	R	$\Delta\phi$ (deg)	D (cm)
1	Port Renfrew	-124.43	48.55	1.16	-9.4	16.63	1.03	-4.94	4.17
2	Sheringham Point	-123.92	48.38	1.19	-16.47	17.95	1	-4.44	4.24
3	Pedder Bay	-123.55	48.33	0.96	-27.39	15.91	0.99	-2.41	2.66
4	Esquimalt	-123.43	48.43	0.91	-23.09	14.40	0.99	-1.04	1.21
5	Victoria	-123.37	48.42	0.89	-17.77	11.62	1.04	-1.83	3.22
6	Clover Point	-123.35	48.41	0.83	-17.95	13.39	1.03	-2.23	3.14
7	Finnerty Cove	-123.3	48.47	0.83	-8.24	9.47	1.02	-2.19	3.25
8	Fulford Harbour	-123.45	48.77	0.82	-3.08	10.78	1	-0.63	0.83
9	Tumbo Channel	-123.11	48.79	1.05	2.03	4.43	1.04	0.66	3.34
10	Patos Island	-122.97	48.78	1.03	0.26	2.32	1.04	-1.5	3.92
11	Whaler Bay	-123.33	48.89	1	-0.76	1.10	1.01	-0.48	1.19
12	Tsawwassen	-123.13	48.99	1	0.92	1.31	1.01	0.19	1.09
13	Sandheads	-123.3	49.1	1.02	-1.05	2.58	1.04	-0.59	3.15
14	Point Grey	-123.27	49.25	0.98	-3.31	5.83	0.96	-0.68	3.63
15	Point Atkinson	-123.25	49.33	1.01	-0.48	1.07	1	-0.56	0.94
16	Gibsons Landing	-123.5	49.4	0.98	0.75	2.34	1	0.96	1.47
17	Winchelsea	-124.08	49.3	1.01	-0.19	0.78	1.01	0.51	1.30
18	Halfmoon Bay	-123.92	49.52	1.01	-0.15	0.83	1.01	0.15	0.72
19	Irvines Landing	-124.05	49.63	1	-0.32	0.59	1.01	0.24	1.12
20	Powell River	-124.55	49.86	1	-1.72	3.05	1	-0.01	0.43
21	Little River	-124.92	49.74	1.03	0.07	2.54	1.01	0.33	0.73
22	Lund	-124.76	49.98	1.02	-2.52	4.98	1.02	-0.95	2.45
23	Twin Islets	-124.93	50.03	1.02	-2.05	4.22	1.01	-0.24	0.72
24	Campbell River	-125.24	50.04	0.99	0.51	1.12	1	0.94	1.39
25	Maude Island E	-125.33	50.13	1.13	-10.02	12.62	0.97	-1.44	2.89
26	Nymphe Cove	-125.36	50.13	1.02	-5.43	6.04	0.97	-0.29	2.02
27	Seymour Narrows	-125.34	50.13	0.63	31.31	53.40	1.14	10.91	17.28
28	Brown Bay	-125.37	50.16	0.98	-5.63	9.26	0.98	-0.04	1.17
29	Chatham Point	-125.44	50.33	1.09	-5.49	12.18	0.98	-3.18	3.85
30	Kelsey Bay	-125.96	50.39	1	-1.69	3.50	0.98	-0.39	1.00
31	Yorke Island	-125.97	50.44	0.99	1.59	3.32	1.01	1.23	1.37
	Mean Error (cm/deg)			4.23	6.5	8.05	1.56	1.49	2.58
	RMS Error (cm/deg)			7.67	10.73	12.73	2.41	2.57	3.91

Table 5: Comparisons of modelled and observed amplitudes and phases. R is the ratio of modelled to observed amplitude. $\Delta\phi$ is the difference between modelled and observed phase. D is the complex difference. The mean error and root mean square (RMS) error are calculated as the difference between the modelled quantity and observed quantity.